Reprinted from

Seventh International Symposium

Machine Processing of

Remotely Sensed Data

with special emphasis on

Range, Forest and Wetlands Assessment

June 23 - 26, 1981

Proceedings

Purdue University
The Laboratory for Applications of Remote Sensing
West Lafayette, Indiana 47907 USA

DIGITAL CORRECTION OF SOLAR ILLUMINATION AND VIEWING ANGLE ARTIFACTS IN REMOTELY SENSED IMAGES

TSUTOMU SHIBATA, WERNER FREI, MARK SUTTON

University of Southern California
Marina del Rey, California

ABSTRACT

We seek to understand and correct shading artifacts caused by varying solar illumination conditions and different viewing angles in remotely sensed images. A synthetic image simulating the shading effects for the sun angle and viewing angle as a real image, is generated using a terrain reflectance model and digital elevation data. A good correlation is obtained between the real and synthetic images. The artifact correction is then made, and a resulting image shows useful information that is not apparent in the original image.

We also present a three-dimensional perspective representation of a terrain with a corresponding aerial photograph mapped on it, which incidentally may help image interpretation.

I. INTRODUCTION

Early successes in digital image change detection suggest many applications of this new technique, notably in remote sensing of the earth surface. The detection of changes in successive aerial photographs permits us for example to monitor ecosystems and discover negative effects at an early stage[1].

Among the difficulties encountered in the change detection are the artifacts caused by changing solar illumination and different viewing angles. The latter effect can typically be seen in a stereo-pair of aerial photographs as shown in Figure 1. These photographs were taken a few seconds apart on the same film with the same exposure, and then developed and digitized in the same batch. As a result, the apparent scene changes in a large area are caused solely by the different viewing angles of a camera mounted on an airplane. This problem is compounded by different sun angles when we compare photographs taken at different times for change detection, as shown in Figure 2. Note that each pair of images of Figures 1 and 2 have been matched geometrically with each other.

In the present study, we have isolated and simulated the effects of sun lighting angle and camera viewing angle to better understand and eventually correct the resulting artifacts. For a given sun angle and camera position, the image intensity is determined as a function of the ground surface gradient which is derived from elevation data. The elevation data used for this study were obtained from topographic maps and respectively consists of an array of 31 x 31 elevations on a 320-foot grid covering a 9920 x 9920 foot region of the Baca area geothermal energy test site in New Mexico, and an array of 31 x 31 elevations on a 550-foot grid covering a 17050 x 17050 foot region of the Geysers area geothermal energy test site in California. Figure 3 shows three-dimensional perspective plots of the elevation data corresponding to the images of Figures 1 and 2, respectively. They show valleys and adjacent mountains which cause shading effects for different sun angles and viewing angles.

The next step is to synthesize a view of the terrain as a function of the above elevations, taking account of reflection properties of the ground surface for a given sun angle and camera position. The synthetic image is then used to remove the shading artifacts from the original (real) image, as described in the following section. Then, we project both the real and the corresponding synthetic images into the same perspective space for comparison. The three-dimensional perspective representation of a terrain with real and synthetic images mapped on it, incidentally, may help image interpretation.

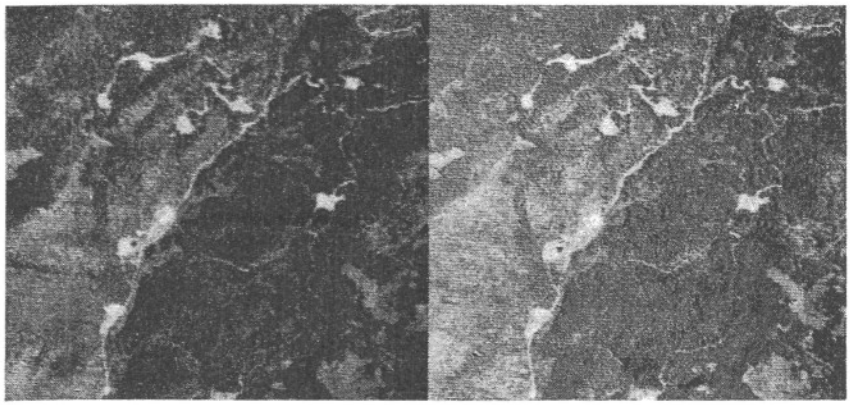

(a) (b)

Figure 1. Digitized pair of stereo aerial photographs of Baca area, New Mexico. Note differences caused solely by the different camera viewing angles. (a) and (b) are registered with each other.

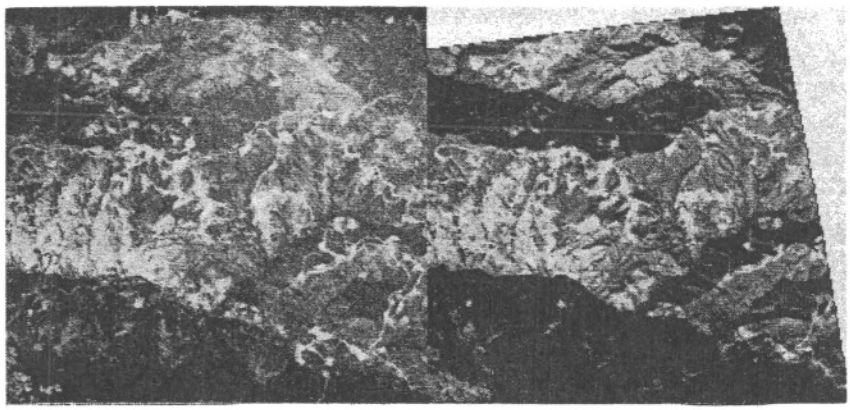

(a) (b)

Figure 2. Digitized pair of successive aerial photographs of Geysers area, California, taken at different times. Note substantial changes caused by different sun angles. (a) and (b) are registered.

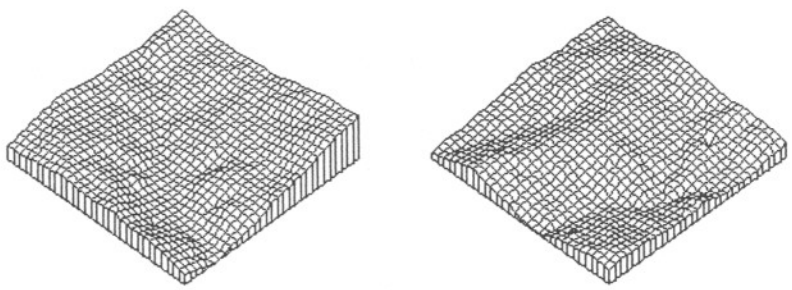

(a) Baca area, New Mexico (b) Geysers area, California

Figure 3. Three-dimensional perspective plots of digital elevation models of Baca area in New Mexico and Geysers area in California.

II. SYNTHETIC IMAGE

Using elevation data and a model of scene reflectance, we can simulate the appearance of the scene for any sun angle and viewing angle. The atomospheric downward and upward scatterings have been assumed small compared to the direct solar irradiation, and shadowing as well as mutual illumination on the ground are temporarily ignored. Referring to the geometry of Figure 4, we determine the sun, camera viewing angle, and surface normal of the local plane in the following way:

A. SUN ANGLE

The solar azimuth and elevation at the latitude of interest at a given time are determined from a diagram in the Smithsonian meteorological tables[2]. The azimuth is measured eastward from north and the elevation is measured upward from the horizon. The unit vector pointing at the sun is then given by

$$\underline{s} = [\sin\phi_s \cos\theta_s, \cos\phi_s \cos\theta_s, \sin\theta_s]$$

B. CAMERA VIEWING ANGLE

The azimuth and elevation of observation of the camera at the location (x,y) are defined in the coordinate system of Figure 4, where the elevation z is expressed as a function of the coordinates x and y. The unit vector pointing at the camera from that location is given by

$$\underline{c} = [\sin\phi_c \cos\theta_c, \cos\phi_c \cos\theta_c, \sin\theta_c]$$

where

$$\cos\phi_c = -y / \sqrt{x^2+y^2}$$

$$\sin\phi_c = -x / \sqrt{x^2+y^2}$$

$$\cos\theta_c = \frac{\sqrt{x^2+y^2}}{\sqrt{x^2+y^2+[ALT - z(x,y)]^2}}$$

$$\sin\theta_c = \frac{ALT - z(x,y)}{\sqrt{x^2+y^2+[ALT - z(x,y)]^2}}$$

and ALT is the altitude of the camera.

C. SURFACE NORMAL OF LOCAL PLANE

The surface gradient consists of two components p and q given by the partial derivatives of the elevation z with respect to x and y, respectively

$$p = \partial z / \partial x$$

$$q = \partial z / \partial y$$

The values of p and q at the location can be approximated by

$$p = [z(x_{i+1},y_j) + z(x_{i+1},y_{j+1}) - z(x_i,y_j) - z(x_i,y_{j+1})] / 2\Delta x$$

$$q = [z(x_i,y_{j+1}) + z(x_{i+1},y_{j+1}) - z(x_i,y_j) - z(x_{i+1},y_j)] / 2\Delta y$$

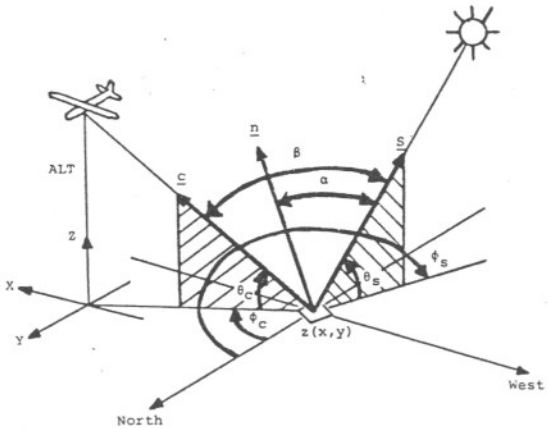

c: Camera observation vector
n: Surface normal vector
S: Sun vector
θ_c: Camera elevation
ϕ_c: Camera azimuth
θ_s: Sun elevation
ϕ_s: Sun azimuth
α: Incident angle
β: Off-backscatter angle
ALT: Altitude of camera

Figure 4. Coordinate System

where Δx and Δy are grid intervals in the x and y directions, respectively. The two slope vectors are then defined as

$$\underline{\ell}_x = (1,0,p)\,\Delta x$$

$$\underline{\ell}_y = (0,1,q)\,\Delta y$$

and if $\Delta x = \Delta y$, the surface normal of the local plane is defined by taking the cross-product of the two slope vectors,

$$\underline{n} = (1,0,p) \times (0,1,q) = (-p,-q,1)$$

D. SIMPLE REFLECTANCE MODEL

Assuming that the terrain has uniform reflectance and ignoring shadowing and mutual illumination, the intensity of light reflected by the surface toward the camera can be expressed by a function of the above three vectors $\underline{s}$, $\underline{c}$, and $\underline{n}$. Assuming also that the surface is an ideal Lambertian reflector (perfect diffuser), the reflectance function R_0 is given by[3]

$$R_0 = \cos\alpha$$

$$= \underline{s} \cdot \underline{n}$$

where α is the incident angle and "$\cdot$" denotes the inner product.

E. THREE-DIMENSIONAL PERSPECTIVE VIEW

For better understanding of the shading effects, we generate three-dimensional perspective views of a terrain with real and synthetic images as follows. The three-dimensional image intensity function $f(x,y,z)$ can be projected onto a two-dimensional perspective plane $f'(x',y')$ by the coordinate transformation,

$$\begin{bmatrix} x' \\ y' \end{bmatrix} = \begin{bmatrix} \cos\phi_o & \sin\phi_o & 0 \\ -\sin\phi_o\cos\theta_o & \cos\phi_o\cos\theta_o & \sin\theta_o \end{bmatrix} \begin{bmatrix} x \\ y \\ z \end{bmatrix}$$

where ϕ_o and θ_o are the azimuth and elevation of a human observer.

Figure 5 shows three-dimensional perspective views of the Geysers area in California, with real and synthetic images mapped on them. To generate the synthetic images simulating the shading effects at different times, the parameters of the solar azimuth and elevation, as well as the camera locations were chosen to correspond to the real images. In figure 5, the real image (a) was taken at 14:46, August 2, 1979, and the sun was at an elevation of 61^o and azimuth of 238^o. While the real image (c) was taken at 13:40, December 11, 1979, and the sun was at an elevation of $25^o$and azimuth of 206^o. The images (b) and (d) are synthetic ones corresponding to (a) and (c), respectively. It is clearly shown that the shading effects are well simulated in the synthetic images. It should be noted again that the different sun angles caused substantial differences in the terrain appearance. The dark regions show reduced solar irradiation due to foreshortening.

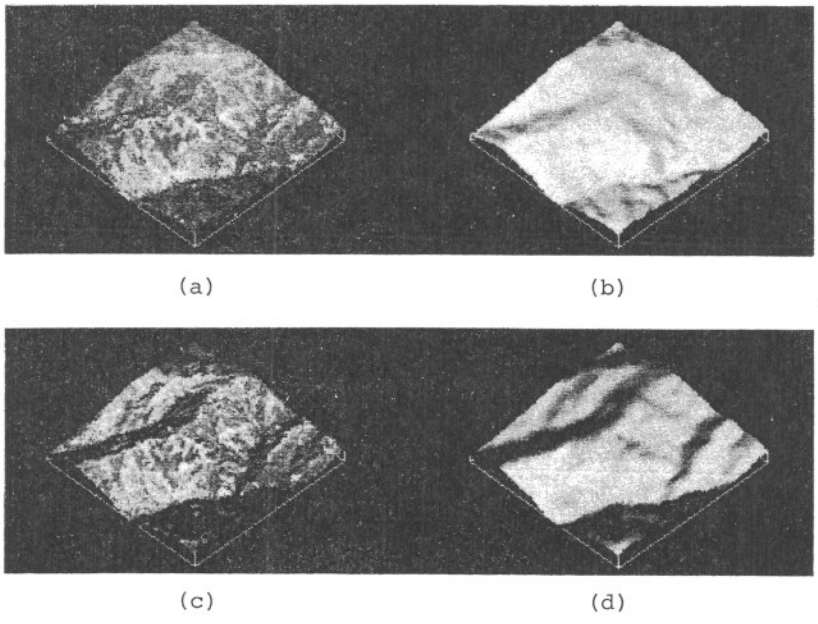

(a) (b)

(c) (d)

(a) Real image of August 2, 1979.

(b) Synthetic image of August 2, 1979.

(c) Real image of December 11, 1979.

(d) Synthetic image of December 11, 1979.

Figure 5. Three-dimensional perspective views of the Geysers area.

III. SHADING CORRECTION

After successfully simulating the shading effects in the synthetic images, next step is to remove the shading artifacts from the real images. A shading correction can be made in a way as shown in Figure 6. Since the elevation data and, consequently the synthetic image has a lower resolution than the corresponding photograhic data, we first generate a low-pass filtered image from the original photographic data (real image) so that the resolution of the two approximately match, while the details (high frequency components) in the original are preserved in a high-pass filtered image. Then, a synthetic image simulating the shading effects is generated using a digital elevation model and a reflectance model for the same sun angle and viewing angle as the photograph. Deshading is performed by subtracting the synthetically shaded image from the low-pass filtered image. The shading correction is then completed by adding the high-pass filtered image to the deshaded image. Note that image intensity is of density mode.

In Figure 7, images (a) and (b) are shading corrected images, image (c) is a change image generated from the original real images (a) and (b) of Figure 2. And image (d) is a shading corrected change image generated from the images (a) and (b) of Figure 7, clearly showing useful information that is not apparent in the change image (c) with no shading corrected.

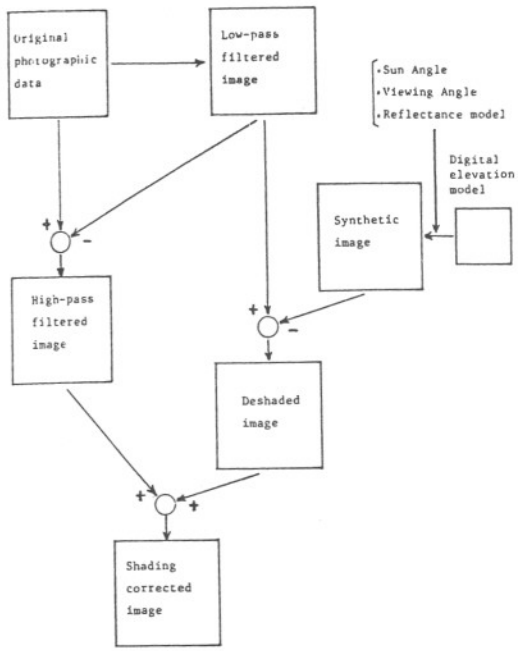

Figure 6. Block diagram for shading correction.

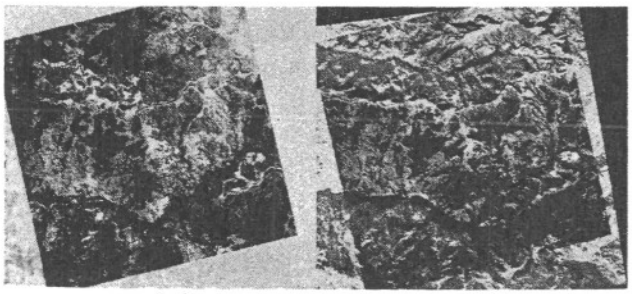

(a) (b)

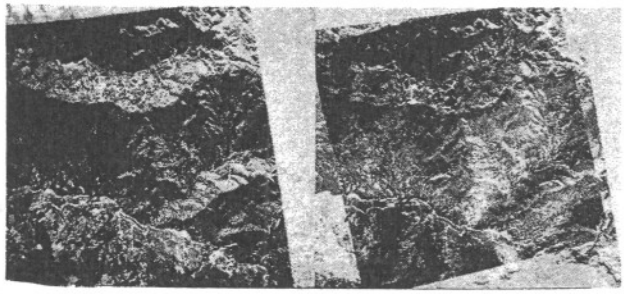

(c) (d)

(a) Shading corrected image of Figure 2-(a).

(b) Shading corrected image of Figure 2-(b).

(c) Change image generated from the images of (a) and (b) of Figure 2, with no shading corrected.

(d) Shading corrected change image generated from the images (a) and (b) of Figure 7, clearly revealing useful information that is not apparent in Figure 7-(c).

Figure 7. Shading corrected image of the Geysers area.

IV. MODELING REFLECTANCE OF NATURAL SURFACE

It has been assumed until now that the earth surface is an ideal Lambertian reflector (perfect diffuser.) Such a surface would appear equally bright from all viewing directions. In fact, the reflectance function R_0 used to produce the synthetic images so far is a function of only the incident angle α , and α is determined by the surface normal and sun angle. This assumption has been used extensively by researchers because of its simplicity, and is not grossly incorrect for certain kinds of remotely sensed data[4]. In our low-altitude aerial photographs however, the different appearances of the terrain from the different viewing directions as shown in the pair of stereo photographs of Figure 1 can not be explained by the simple Lambertian surface reflectance model. In fact, the reflectance characteristics of most natural surfaces are anisotropic[5]. We therefore propose here a more sophisticated and realistic reflectance function for natural surfaces, taking account of both the forwardscatter and backscatter, as well as the diffuse reflection. This new reflectance function R_1 is given by

$$R_1 = \{k_1+(1-k_1)[(k_2\cos^m\gamma+(1-k_2)\cos^n\beta]\}\cos\alpha$$

where

$$\cos\alpha = \underline{s}\cdot\underline{n}$$

$$\cos\beta = \underline{s}\cdot\underline{c}$$

$$\cos\gamma = 2\,(\underline{s}\cdot\underline{n})\,(\underline{c}\cdot\underline{n}) - (\underline{s}\cdot\underline{c})$$

and

- k_1 is the surface diffuse reflection coefficient
- k_2 is the surface forwardscatter coefficient
- m is a power which models the forwardscatter
- n is a power which models the backscatter

These coefficients must be empirically adjusted for each image, and physical justification can be made based on the reflection properties of the corresponding natural surface when they are known.

Figure 8 illustrates two- and three-dimensional perspective representations of this new reflectance function for $k_1 = 0.3$, $k_2 = 0.3$, $m = 30$, and $n = 30$.

For a pair of stereo photographs such as shown in Figure 1, if we can assume that the difference in intensity between corresponding elements of the two real images A and B can be expressed by a function of the off-backscatter angles β_A and β_B such that

$$f_A(x,y) - f_B(x,y) = g(\beta_A,\beta_B)$$

we can make the correction for one photograph with reference to the other (relative correction.) The above assumption is based on measurements reported elsewhere, which indicate much stronger backscatter than forwardscatter or diffuse reflection in vegetated surfaces[6]. We then model $g(\beta_A,\beta_B)$ such that

$$g(\beta_A,\beta_B) = \cos\beta_A - \cos\beta_B$$

and linear regression is used to find the best fit line between $f_A(x,y) - f_B(x,y)$ and $\cos\beta_A - \cos\beta_B$.

Figure 9 shows a shading corrected stereo pair of the photographs of Figure 1, and the shading is corrected for image (a) with reference to image (b). Now each pair of corresponding elements in the two images appear to have almost the same intensity. In other words, the shading artifacts have been successfully corrected.

Figure 10 summarizes the three-dimensional perspective representaion of a terrain with a corresponding photagraph mapped on it. In figure 10, (a) is a digitized aerial photograph of Baca area, New Mexico. (b) is a three-dimensional perspective plot of digital elevation model corresponding to the area covered by the photograph (a). (c) is a three-dimensional perspective view of the Baca area with the aerial photograph mapped on it. Note that perspective view from any viewing direction can be generated.

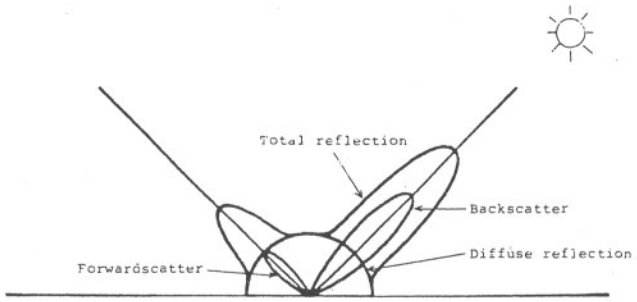

(a) Two-dimensional representation of the reflectance model.

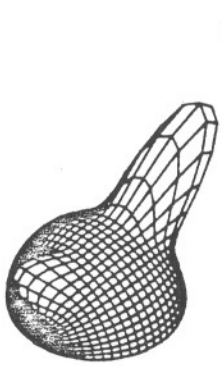

(b) Three-dimensional representation of the reflectance model.

Figure 8. Indicatrix of proposed new surface reflectance model.

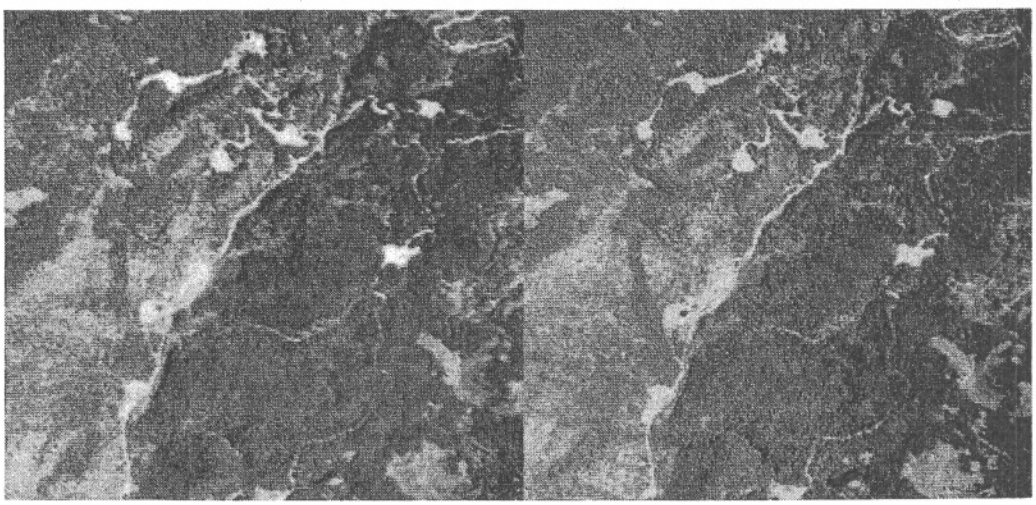

(a)
Shading corrected image of Figure 1-(a) with reference to the image of Figure 1-(b), showing considerable improvement.

(b)
The same image as Figure 1-(b), shown again here for comparison.

Figure 9. Shading corrected pair of the stereo images of Figure 1.

(a)

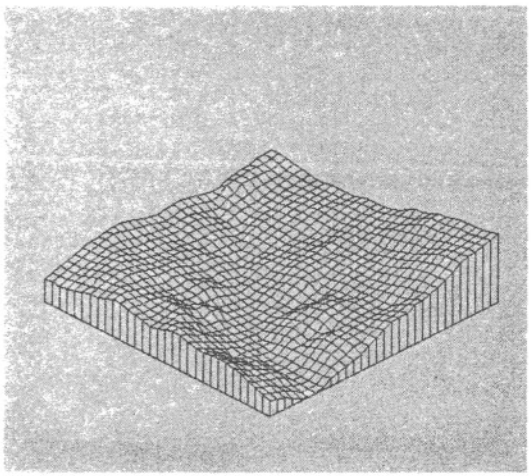

(b)

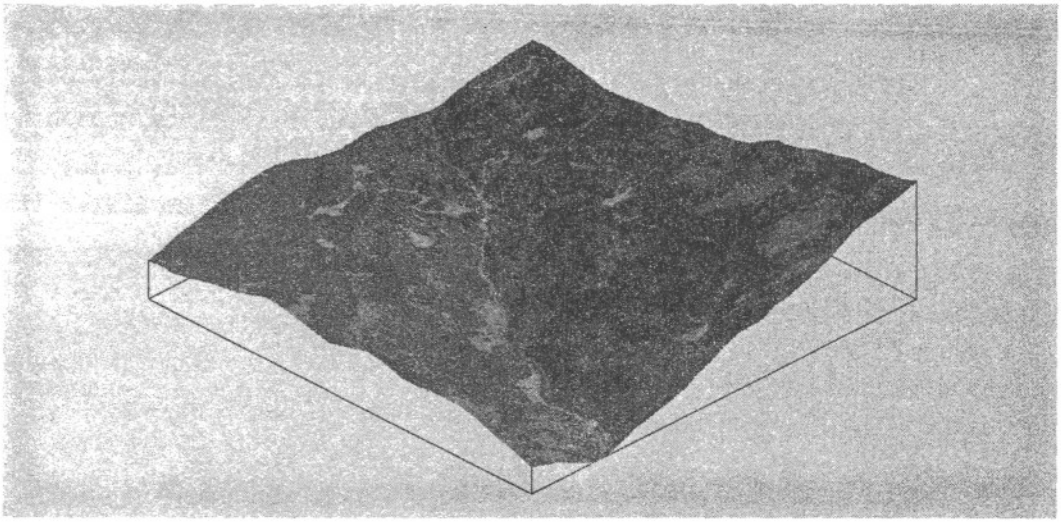

(c)

(a) Digitized aerial photograph of the Baca area, being matched geometrically with digital elevation model.

(b) Three-dimensional perspective plot of digital elevation model corresponding to the area covered by the photograph (a).

(c) Three-dimensional perspective view of the Baca area with the aerial photograph of (a) mapped on it. Note that perspective view from any viewing direction can be generated.

Figure 10. Three-dimensional perspective representation of terrain.

V. CONCLUSIONS

We have simulated and corrected the shading artifacts caused by varying solar illumination conditions and different viewing angles in remotely sensed images for more accurate image change analysis and interpretation. The artifacts correction clearly reveals useful information that was not apparent in the original images. Since natural scenes usually consist of many different types of surfaces, further work is currently under way to incorporate texture factors and classification of surface type into our reflectance mode for better correction.

We have also demonstrated the usefulness of the three-dimensional perspective representation of a terrain with a corresponding aerial photograph mapped on it for better image interpretation.

ACKNOWLEDGEMENTS

The research reported in this paper was supported by the Department of Energy under contract #DE-AS03-76-SF00113.

REFERENCES

1. W. Frei, M. Singh, and T. Shibata, "Digital Image Change Detection", Optical Engineering, Vol. 19, No. 3, May/June 1980.

2. R.J. List (ed), "Smithsonian Meteorological Tables", Smithsonian Institute, Washington, D.C., 1951.

3. B.K.P. Horn and B.L. Bachman, "Using Synthetic Images to Register Real Images with Surface Models", Comm. ACM, Vol. 21, No. 11, November 1978.

4. C.J. Robinove and P.S. Chavez, "LANDSAT Albedo Monitoring for An Arid Region", The AAAS International Symposium on Arid Region Plant Resources, Lubbock, Texas, October 1978.

5. B. Brennan and W.R. Bandeen, "Anisotropic Reflectance Characteristics of Natural Earth Surfaces", Applied Optics, Vol. 9, No. 2, February 1970.

6. F.D. Eaton and I. Dimhirn, "Reflected Irradiance Indicatrices of Natural Surfaces and Their Effect on Albedo", Applied Optics, vol. 18, No. 7, April 1979.

AUTHOR BIOGRAPHICAL DATA

Tsutomu Shibata received the B.S. degree from Nihon University, Japan, and the M.S. degree from Kagoshima University, Japan, both in electrical engineering, in 1970 and 1972, respectively. He worked in image processing and pattern recognition systems development as a Research Engineer at the Matsushita Research Institute Tokyo, Inc. (Panasonic Japan). He is currently a Visiting Assistant Professor of Radiology, Medical Imaging Science Group, University of Southern California. His research interests include remote sensing, scene analysis, medical image processing, computer graphic, and visual perception.

Werner Frei received the B.S. degree in 1968 and the Ph.D. degree in 1972 in electrical engineering from the Federal Institute of Technology, Zurich, Switzerland. He was an Assistant Professor at the University of Southern California in the Department of Electrical Engineering, and a staff member at the USC Image Processing Institute. There, his research was directed toward digital image coding and processing, as well as related phenomena of visual perception. In 1976, he joined the faculty of the USC Medical School, where he is now Associate Director of the Medical Imaging Science Group in the Department of Radiology. He is in charge of the digital image analysis research effort pursued by the group.

Mark D. Sutton is a student at the University of Southern California majoring in electrical engineering. He works at USC Medical Imaging Science Group as a programmer and has worked on system programming, image registration, and hill shading. His interests include systems hardware and software design, sound synthesis using computers, and computer genarated animation.